Intestinal microbiota control acute kidney injury severity by immune modulation

Jihyun Yang[1], Chan Johng Kim[2], Yoon Sook Go[1], Hee Young Lee[1], Myung-Gyu Kim[1], Se Won Oh[1], Won Yong Cho[1], Sin-Hyeog Im[2] and Sang Kyung Jo[1]

[1]*Division of Nephrology, Department of Internal Medicine, Korea University Medical College, Seoul, Korea; and* [2]*Division of Integrative Biosciences and Biotechnology & Department of Life Sciences, Pohang University of Science and Technology (POSTECH), Pohang, Republic of Korea*

Intestinal microbiota impacts the host immune system and influences the outcomes of chronic diseases. However, it remains uncertain whether acute kidney injury (AKI) impacts intestinal microbiota or vice versa. To determine this, we investigated the mechanistic link between AKI, microbiota, and immune response in ischemia/reperfusion injury. Microbiota alteration and its biological consequences after ischemia/reperfusion injury were examined and the effect of dysbiotic microbiota on the outcome of AKI was also assessed by colonizing germ-free mice with post-AKI microbiota. The role of Th17, Th1, Tregs cells and macrophage polarization in mediating the renoprotective effect of antibiotic induced microbiota depletion in ischemia/reperfusion injury was also determined. Increase of *Enterobacteriacea*, decrease of *Lactobacilli*, and *Ruminococacceae* were found to be the hallmarks of ischemia/reperfusion injury induced dysbiosis and were associated with a decreased levels of short-chain fatty acids, intestinal inflammation and leaky gut. Colonizing germ-free mice with post-AKI microbiota worsened ischemia/reperfusion injury severity with exaggerated inflammation in recipient mice compared to colonizing with microbiota from sham operated mice. Microbiota depletion by oral antibiotics protected against ischemia/reperfusion injury. This renoprotective effect was associated with reduced Th 17, Th 1 response along with expansion of regulatory T cells, and M2 macrophages. Our study demonstrated a unique bidirectional relationship between the kidney and the intestine during AKI. Intestinal dysbiosis, inflammation and leaky gut are consequences of AKI but they also represent an important modifier determining post-AKI severity. Thus, targeting the intestinal microbiota might provide a novel therapeutic strategy in AKI.

Correspondence: *Sang Kyung Jo, Department of Internal Medicine, Division of Nephrology, Korea University Medical College, Korea University Anam Hospital, Koreadae-Ro 73, Sungbuk-Gu, Seoul, Republic of Korea 02841. E-mail: sang-kyung@korea.ac.kr; or Sin-Hyeog Im, Division of Integrative Biosciences and Biotechnology & Department of Life Sciences, Pohang University of Science and Technology (POSTECH), Chungam-Ro 77, Nam-Gu, Pohang, Kyungsangbuk-Do, Republic of Korea 37673. E-mail: iimsh@postech.ac.kr*

Received 28 August 2019; revised 13 March 2020; accepted 13 April 2020; published online 26 May 2020

Kidney International (2020) ■, ■–■; https://doi.org/10.1016/j.kint.2020.04.048

KEYWORDS: acute kidney injury; dysbiosis; ischemia/reperfusion; leaky gut; macrophages; short-chain fatty acids; T cells

Translational Statement

This study demonstrates a unique bidirectional relationship between the kidney and intestine during acute kidney injury. Acute kidney injury provokes intestinal dysbiosis, T helper cell 17, neutrophil, and M1 macrophage mediated intestinal inflammation as well as leaky gut with bacterial translocation. Dysbiotic microbiota transferred to germ-free mice aggravated kidney injury. Depletion of microbiota before injury partially mitigated kidney injury, and the renoprotective effect is associated with significantly reduced T helper cell 1, T helper cell 17 response and expansion of regulatory T cells, and M2 macrophages. Targeting the intestine might provide novel strategies for the prevention and treatment of acute kidney injury.

Despite progress in understanding the pathogenesis of acute kidney injury (AKI), the mortality of dialysis requiring AKI still remains high.[1–3] Uremic complications and AKI-induced distant organ dysfunction might contribute to this worse outcome,[4,5] However, compared with lung and heart, little is known about the interaction between the kidney and intestine.

The intestine harbors over 100 trillion commensal bacteria.[6,7] Emerging evidence indicates that intestinal dysbiosis is associated with many inflammatory, metabolic diseases.[7–12] Studies shed light on kidney–intestine crosstalk in AKI. Park *et al.*[13] demonstrated that ischemia/reperfusion injury (IRI) induced the release of interleukin (IL)-17A from the small intestine, mediating intestinal and hepatic injury. Another study by Andrade-Oliveira *et al.*[14] also suggested kidney–intestine crosstalk by showing that short-chain fatty acids (SCFAs) prevented IRI. However, none of these studies demonstrated a direct link between microbiota and AKI.

The intestine is the single largest organ of the immune system, and contribution of microbiota and mucosal immune cells to local inflammatory conditions such as inflammatory bowel disease is well known.[15] However, recent studies show that these are potent regulators of systemic immunity as well, and they could also control extraintestinal biologic functions.[16,17] Given that overwhelmed activation of innate immune response is important in the pathogenesis of AKI, there is a possibility that microbiota alteration and intestinal mucosal immunity might impact AKI outcome.

In this study we examined whether microbiota could affect the post-AKI outcome by modulating immune response in kidney IRI. We showed that IRI-induced dysbiosis led to significantly altered metabolic, immunologic, and barrier functions of the intestine. At the same time we also observed AKI-induced dysbiosis negatively affected post-AKI outcome by showing germ-free (GF) mice colonized with post-IRI microbiota developed more severe injury in recipient mice. Depletion of microbiota before injury resulted in marked protection against renal IRI, and this renoprotective effect was partially mediated via reduction of T helper cell 17 (Th17), T helper cell 1 (Th1) response and also expansion of regulatory T cells (Tregs), and M2 macrophages. Collectively, these data suggest that intestinal microbiota and mucosal immunity might control kidney inflammation and injury and can be important modifiers of AKI outcome. Targeting intestinal microbiota could provide a novel strategy in the treatment of AKI.

RESULTS

Kidney IRI induces intestinal dysbiosis

To assess the impact of IRI on intestinal microbiome, we performed 16S rRNA gene sequencing analysis of mice feces from sham, IRI day 1, and bilateral nephrectomy. The number of operational taxonomic units (OTUs), species richness estimates (Chao1 and abundance-based coverage estimator (ACE), and species diversity index (Shannon) showed no difference between the 3 groups (Figure 1a). However, the microbial community of IRI or nephrectomized mice was clearly distinguished from the sham group in principal coordinate analysis (Figure 1b). Hallmarks of kidney IRI-induced dysbiosis included relative increases of *Escherichia* and *Enterobacter* and relative decreases of *Lactobacillus,* Ruminococcaceae, *Faecalibacterium,* and *Lachnospiraceae* (Figure 1c).

Biologic consequences of kidney IRI-associated intestinal dysbiosis

After kidney IRI, the numbers of neutrophils and macrophages increased significantly in the colon, suggesting the development of intestinal inflammation (Figure 2a). Among the colon macrophage subset, expansion of $CX_3CR_1^{int}$ $Ly6c^+$ proinflammatory macrophage was prominent with increased expression of inducible nitric oxide synthase (iNOS) and decreased expression of arginase, suggesting that macrophage polarization shifted to proinflammatory M1 phenotype in the colon after kidney IRI (Figure 2b and c). Intracellular cytokine staining of lymphocytes showed that dysbiosis is also associated with expansion of $IL\text{-}17A^+$ CD4 cells in both small and large intestine, suggesting the important role of Th17 pathways in kidney IRI-induced intestinal inflammation (Figure 2d).

We also observed that intestinal permeability significantly increased along with increased endotoxin level (Figure 3a and b). The actual number of amplicon reads of bacterial 16S rRNA of liver in day 1 IRI also showed a significant increase compared with sham-operated mice (Figure 3c). Despite the inadequate number of the amplicon reads for assigning subsequent OTU analysis, these data could suggest the development of bacterial translocation after kidney IRI. Significantly decreased claudin-1 increased claudin-2 (Figure 3d), and increased numbers of apoptotic colonocytes (Figure 3e) are likely to contribute to barrier disruption and subsequent bacterial translocation after AKI. IRI-induced dysbiosis was also associated with significantly decreased levels of SCFAs in feces (Figure 3f).

Dynamic changes of intestinal microenvironment after kidney IRI

The microbial structure during the recovery phase of IRI on days 3 and 7 was clearly distinguished from that of day 1 IRI and characterized by partial restoration of the relative abundance of genus *Lactobacilli* (Figure 4a–c). In line with this change of microbiome, the level of stool butyrate was also partially restored on IRI day 7 (Figure 4d). Significantly increased neutrophils in the colon of day 1 IRI also returned to baseline, whereas colon macrophage or apoptotic colonocytes remained elevated (Figure 4e).

Intestinal dysbiosis is causally linked to severity of IRI

Although intestinal dysbiosis is known to be involved in many pathologic processes, it remains unclear whether AKI-associated intestinal dysbiosis directly contributes to the pathogenesis of kidney IRI. To determine whether post-IRI dysbiosis has an impact on AKI severity, we used a microbiota transfer model in GF mice. We reconstituted GF mice with fecal microbiota from sham-operated or IRI mice and then underwent kidney IRI on the recipient mice. Mice who received microbiota from IRI mice developed more severe injury compared with those that received microbiota from sham-operated mice. Blood urea nitrogen, serum creatinine, and tubular injury scores were significantly higher in GF mice with microbiota reconstitution from IRI mice (Figure 5a and b). Next, we analyzed inflammatory cytokine concentrations in the post-ischemic kidneys and observed that recipients of post-IRI microbiota exhibited significantly higher levels of kidney tumor necrosis factor (TNF)-α and interferon (IFN)-γ mRNA compared with sham recipients (Figure 5c). These data suggest that dysbiotic microbiota after kidney IRI aggravated inflammation and directly contribute to the severity of kidney injury.

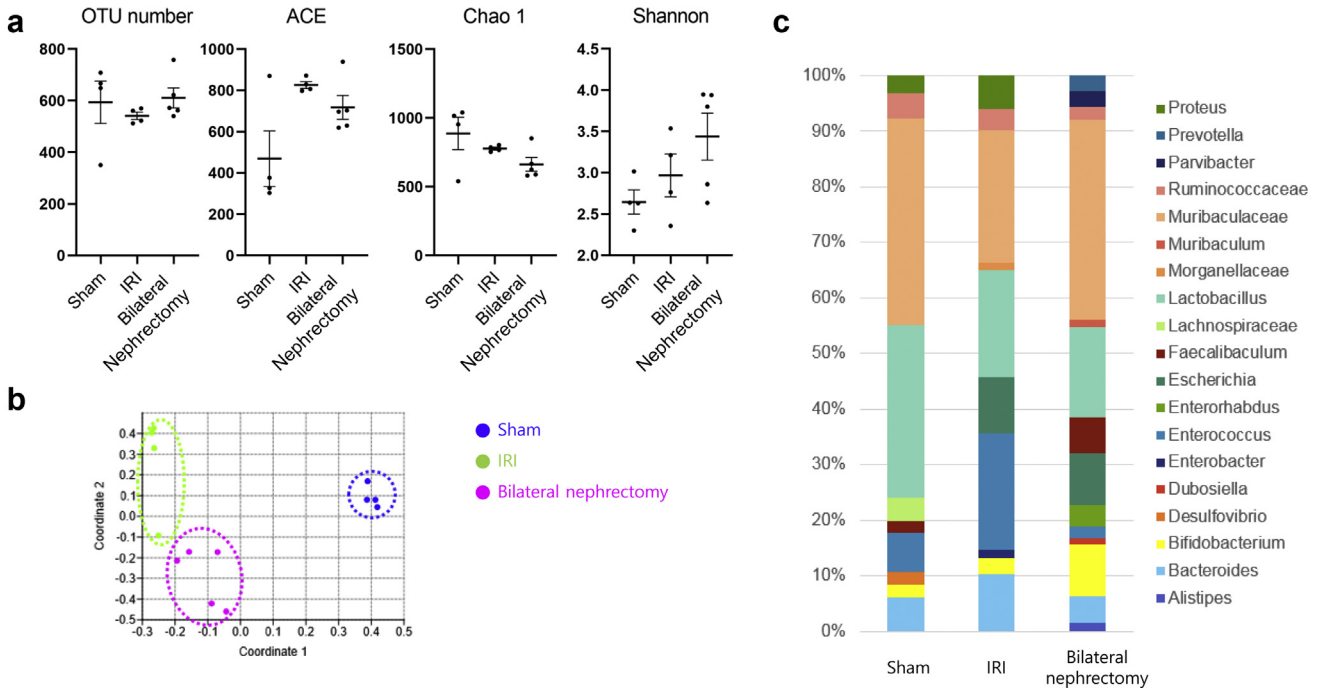

Figure 1 | Acute kidney injury–induced dysbiosis. Fecal samples obtained in sham-operated, day 1 ischemia/reperfusion injury (IRI), and bilateral nephrectomized mice were analyzed. (**a**) Quantitative analysis of microbiome showing the species richness (number of operational taxonomic units [OTUs], abundance-based coverage estimator [ACE], Chao 1) and species diversity (Shannon) in sham, IRI day 1, and bilateral nephrectomized mice. (**b**) Principal coordinate analysis of intestinal microbiome by taxonomic abundance pattern in sham, IRI day 1, and bilateral nephrectomized mice. (**c**) Only genera with a frequency >1% and with statistically significant differences between the groups were included. Four to 5 per group.

Depletion of intestinal microbiota is protective in kidney IRI

Based on our data, we hypothesized that intestinal microbiota might be a novel therapeutic target in kidney IRI, so we tested the effect of microbiota depletion. Oral administration of an antibiotic combination for 2 weeks before IRI resulted in marked decrease of OTUs (data not shown), and antibiotic-induced microbiota depletion (AIMD) conferred a significant renoprotective effect against IRI. Serum creatinine, tubular injury, and the number of kidney infiltrating neutrophils or macrophages decreased significantly (Figure 6a and b). Levels of monocyte chemoattractant peptide-1 and IL-6 also decreased, indicating decreased inflammation (Figure 6c). AIMD also resulted in decreased colonocyte apoptosis, colon inflammation, restoration of claudin-1 and -2 expression, and permeability (Supplementary Figure S1).

Protective effect of AIMD is partially mediated by decreased Th1, Th17 response and expansion of Tregs, and M2 macrophages

Next, we sought to elucidate mechanisms of protection exerted by AIMD. Because the intestine is the largest reservoir of T cells in our body and microbiota is important in shaping the immune response, we tested whether these cells contribute to the beneficial effect of AIMD in kidney IRI. First, we examined mesenteric lymph node (MNL) T-cell function. T cells from MNLs from AIMD mice showed a significantly reduced proliferative response on anti-CD3 and anti-CD28 co-stimulation determined by bromodeoxyuridine (BrdU) incorporation (Figure 7a). In addition, we observed that the renoprotective effect of AIMD was associated with significantly reduced Th17 and Th1 response in the small intestine and also with the expansion of $CD4^+$ $CD25^+$ Tregs, and Foxp3 expression in MNL, spleen, and kidneys of IRI mice (Figure 7b and c). Depletion of Tregs by administration of anti-CD25 monoclonal antibodies and adoptive transfer of $Foxp3^+$ cells in Treg depleted AIMD mice resulted in partial loss and restoration of the protective effect of AIMD in kidney IRI (Figure 7d). Finally, to exclude the direct effect of antibiotics on Treg expansion, MNL cells were co-cultured with antibiotic combinations. There was no difference in percentage of Tregs, suggesting that antibiotic-induced Treg expansion might be mediated by their effect on microbiota (Figure 7e).

In addition, we also tested whether the renoprotective effect of AIMD was partially mediated by macrophage polarization. We measured the percentage of $Ly6G^{low}CX_3CR_1^{high}$ resident macrophages in the colon; those were significantly increased after IRI in AIMD mice (Figure 8a). Reverse transcriptase-polymerase chain reaction (PCR) analysis of iNOS and arginase also suggest that these cells represent M2-like macrophages (Figure 8b). AIMD also led to increased $CD206^+$ $F4/80^+$ M2 macrophages in post-ischemic kidneys with decreased iNOS and increased arginase expression (Figure 8c and d). Given that M2 macrophages exert an anti-

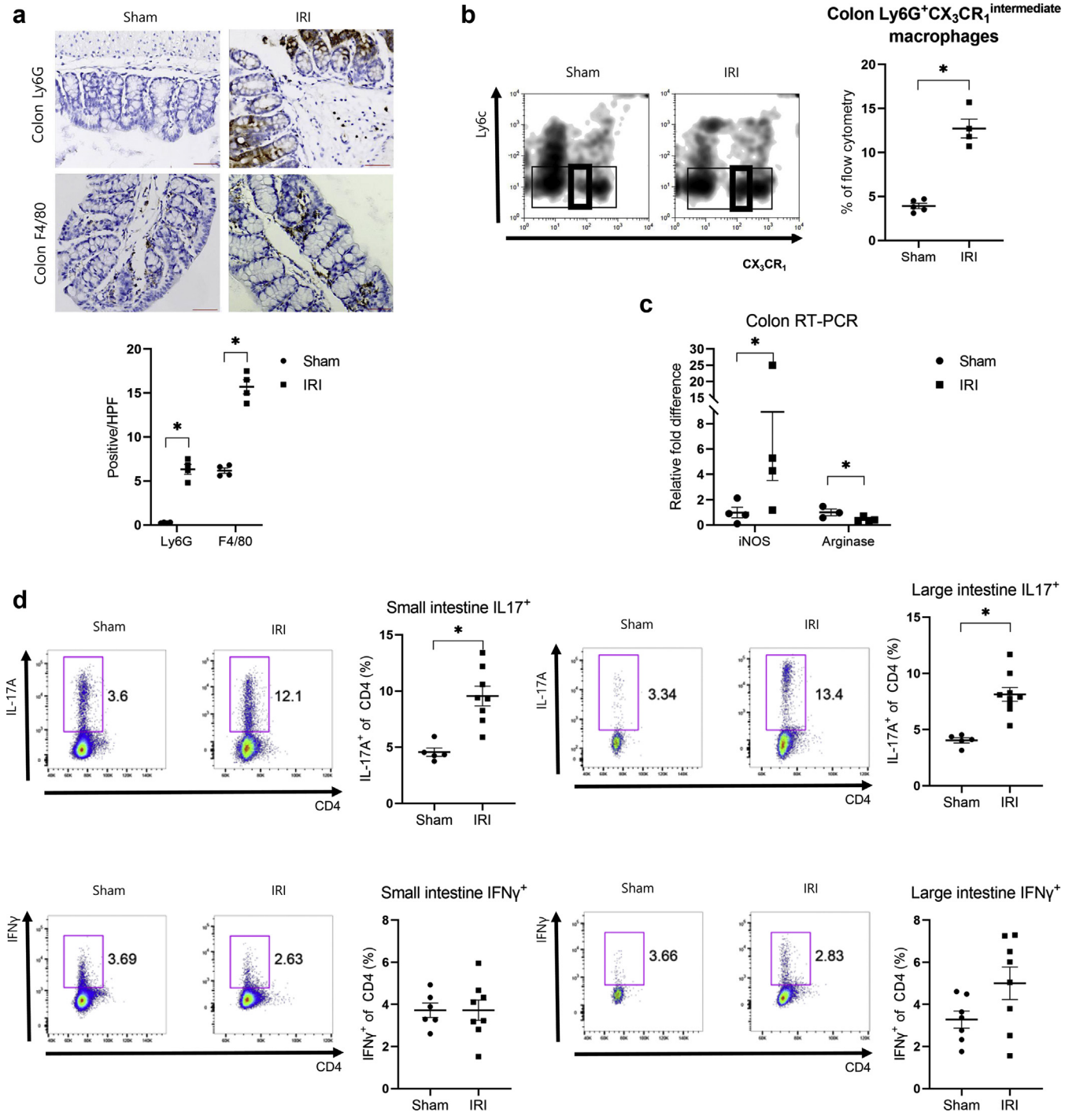

Figure 2 | Kidney ischemia/reperfusion injury (IRI)–induced dysbiosis is associated with intestinal inflammation. (**a**) Colon inflammation. Representative images are Ly6G^{+} neutrophils and F4/80^{+} macrophages in the colon of sham and day 1 of IRI. The number of positive cells per high power fields (HPFs) was compared. Original magnification ×200. (**b**) Flow cytometric analysis of colon Ly6c^{+}CX$_3$CR$_1^{+}$ macrophages in sham and day 1 of IRI. Percentage of Ly6c^{low} CX$_3$CR$_1^{intermediate}$ proinflammatory macrophages was determined. (**c**) Reverse transcriptase-polymerase chain reaction (RT-PCR) analysis of colon-inducible nitric oxide synthase and arginase. Relative fold difference compared with sham-operated mice were compared. (**d**) Flow cytometric detection of interleukin (IL)-17A^{+} or interferon (IFN)-γ^{+} CD4 cells in small and large intestines in sham and day 1 of IRI. Symbols represent individual animals, and horizontal lines show mean values. Data are expressed as mean ± SEM. The 2-tailed unpaired *t* test was used in all graphs (5–8 per group). *$P < 0.05$ compared with the sham. To optimize viewing of this image, please see the online version of this article at www.kidney-international.org.

inflammatory effect, these results suggest that AIMD-induced M2 macrophage polarization in both colon and kidney might partially contribute to a renoprotective effect of AIMD.

DISCUSSION

Our study demonstrated a novel, bidirectional relationship between the kidney and intestine during AKI. Kidney IRI

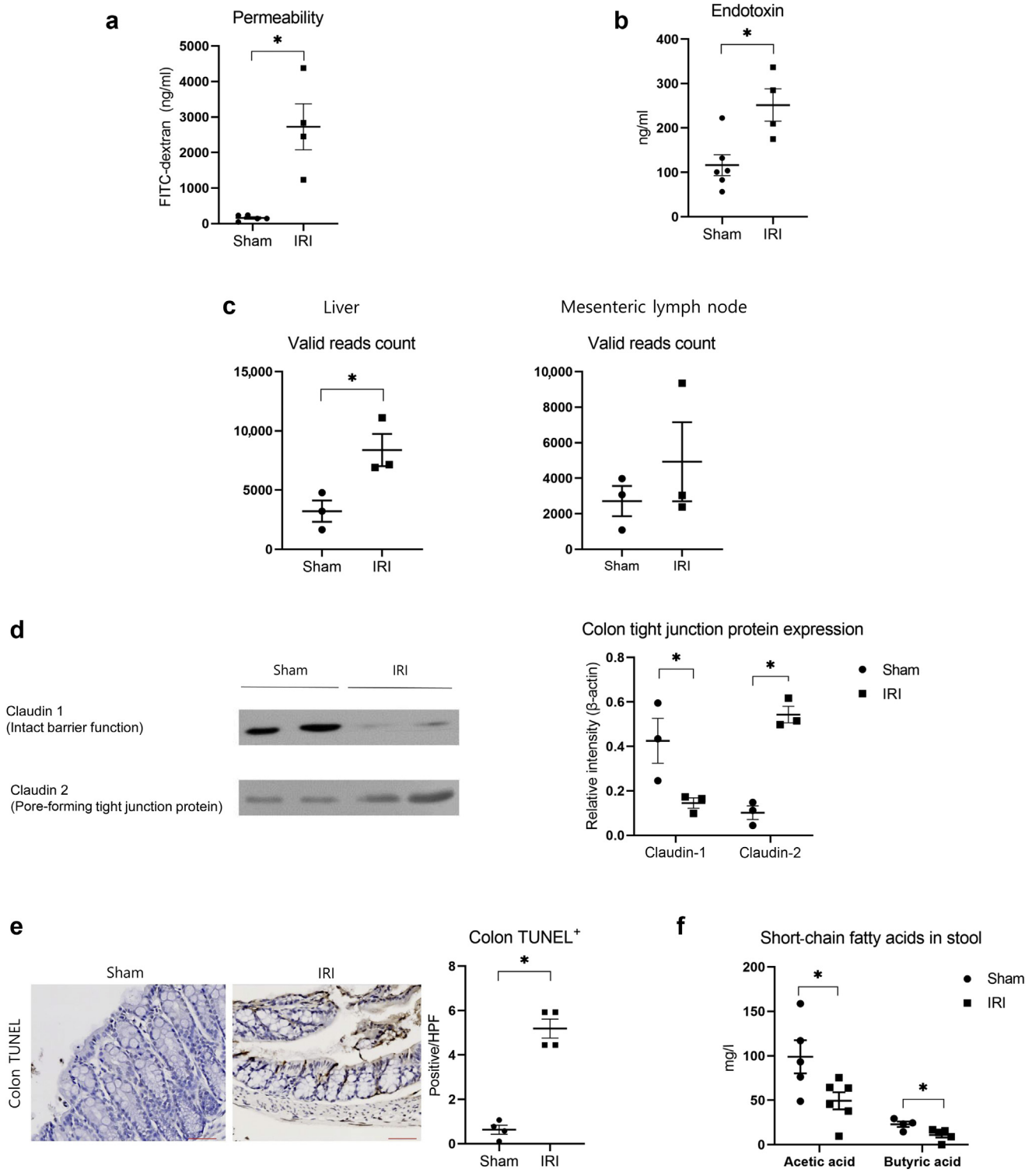

Figure 3 | Kidney ischemia/reperfusion injury (IRI)–induced dysbiosis is associated with increased permeability and bacterial translocation. (**a**) Intestinal permeability was measured by detecting fluorescein activity of fluorescein isothiocyanate conjugated (FITC) 4 hours after oral administration of FITC-dextran in sham and day 1 of IRI. (**b**) Serum endoxin level in sham and day 1 of IRI. (**c**) Quantitative analysis of microbiome showing the number of valid amplicon reads in mesenteric lymph nodes and liver tissues in sham and day 1 of IRI. (**d**) Band intensities of claudin-1 and claudin-2 normalized to β-actin in Western blots were compared. (**e**) Representative images are deoxynucleotidyl transferase dUTP nick end labeling (TUNEL) stain of colon in sham and day 1 of IRI, the number of TUNEL positive cells per high-power field (HPF; original magnification ×200) was compared. (**f**) Levels of acetic acid and butyric acid in feces in sham and day 1 after IRI. Symbols represent individual animals, and horizontal lines show mean values. Data are expressed as mean ± SEM. The 2-tailed unpaired *t* test was used in all graphs (4–5 per group). *$P < 0.05$ compared with the sham group. To optimize viewing of this image, please see the online version of this article at www.kidney-international.org.

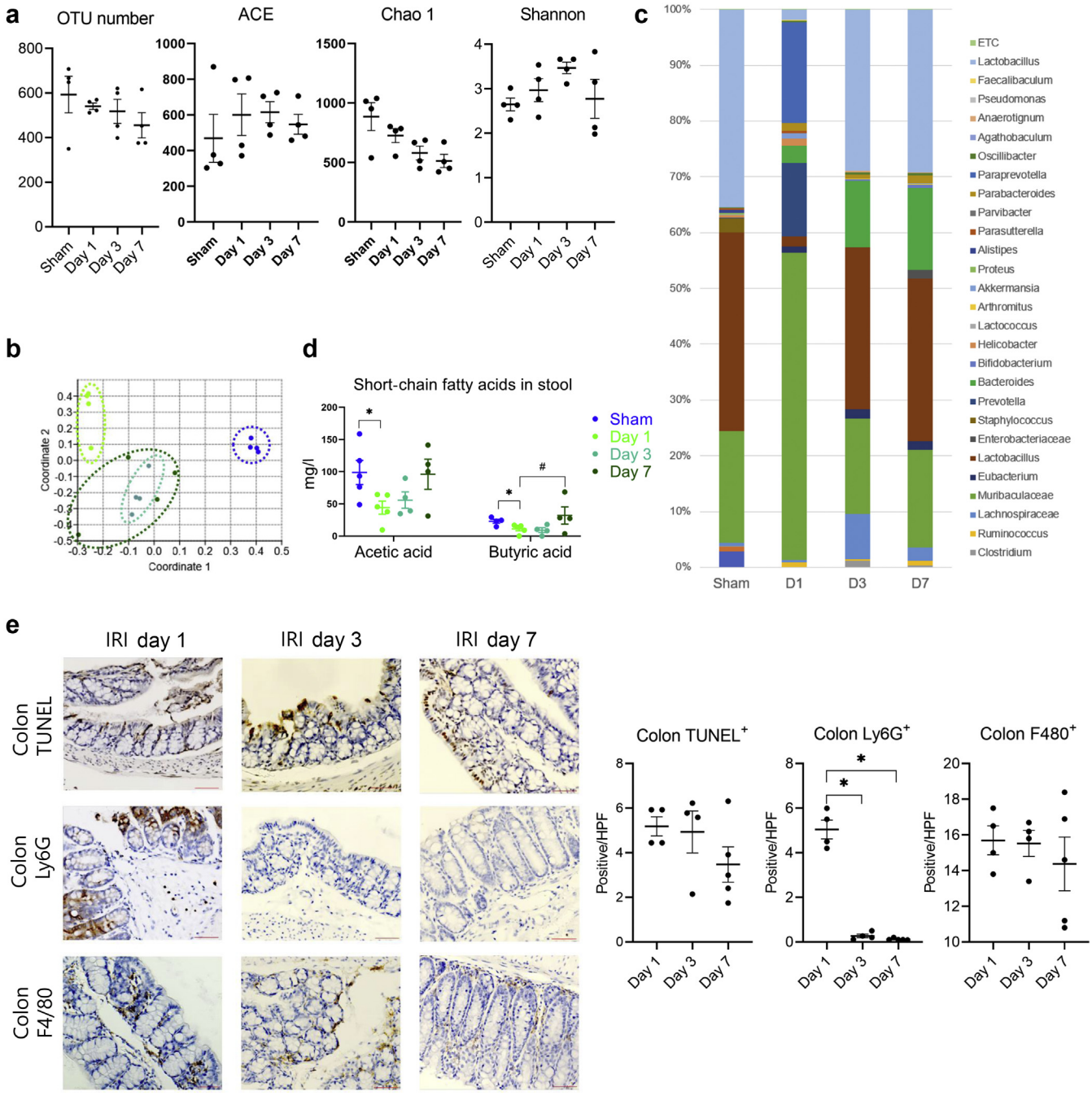

Figure 4 | Dynamic changes of intestinal microbiome, inflammation, and metabolites after ischemia/reperfusion injury (IRI). (**a**) Fecal samples obtained in sham, days 1, 3, and 7 after IRI were analyzed. Quantitative analysis of microbiome showing the species richness (number of operational taxonomic units [OTUs], abundance-based coverage estimator [ACE], Chao 1) and species diversity (Shannon) in sham IRI days 1, 3, and 7. (**b**) Principal coordinate analysis of intestinal microbiome by taxonomic abundance pattern in sham, IRI days 1, 3, and 7. (**c**) Only genera with a frequency >1% and with statistically significant differences between the groups were included. (**d**) Levels of acetic acid and butyric acid in feces in sham, days 1, 3, and 7 of IRI. (**e**) Deoxynucleotidyl transferase dUTP nick end labeling $(TUNEL)^+$ colonocyte apoptosis, $Ly6G^+$ neutrophils, $F4/80^+$ macrophages in the colon on days 1, 3, and 7 of IRI, original magnification ×200. Symbols represent individual animals, and horizontal lines show mean values. Data are expressed as mean ± SEM. The 2-tailed unpaired *t* test was used in all graphs (4–5 per group). $^*P < 0.05$ compared with the sham. $\#P < 0.05$ day 1 versus day 7. To optimize viewing of this image, please see the online version of this article at www.kidney-international.org.

profoundly altered the intestinal microbiota with barrier disruption, bacterial translocation, and metabolic, immune dysfunction. This dysbiosis subsequently worsened kidney injury by augmenting inflammation. We also demonstrated that depletion of microbiota protected against IRI, and this renoprotective effect was partially

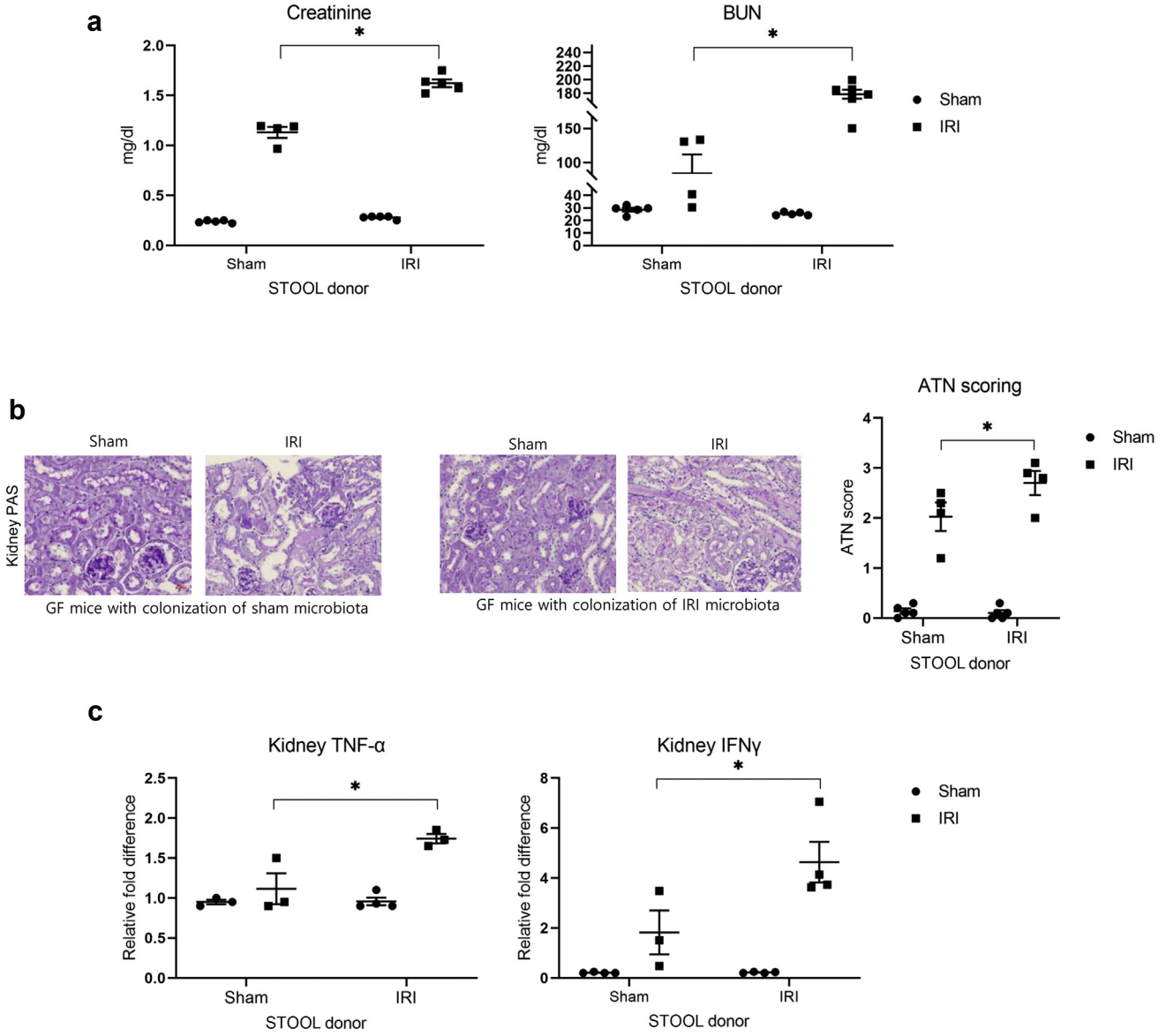

Figure 5 | Ischemia/reperfusion injury (IRI)–induced dysbiosis affect after acute kidney injury inflammatory response and exacerbate outcome. Germ-free (GF) mice were colonized by microbiota from post-IRI or sham-operated mice and underwent 28 minutes and 30 seconds of clamping of bilateral renal pedicles. Mice were sacrificed on day 1. (**a**) Serum creatinine and blood urea nitrogen (BUN) level on day 1 after IRI. (**b**) Representative images of periodic acid–Schiff (PAS)–stained kidney sections of GF mice colonized by microbiota from sham-operated and post-IRI mice that underwent sham or kidney IRI, day 1, original magnification ×100, PAS. Tubular injury score. (**c**) Reverse transcriptase-polymerase chain reaction analysis of tumor necrosis factor α (TNF-α) and interferon γ (IFN-γ) expression in kidney tissues and relative fold difference compared with sham-operated GF mice were compared. Symbols represent individual animals, and horizontal lines show mean values. Data are expressed as mean ± SEM. The 2-tailed unpaired *t* test was used in all graphs (4–5 per group) $^*P < 0.05$ compared with GF IRI mice colonized by sham microbiota. To optimize viewing of this image, please see the online version of this article at www.kidney-international.org.

mediated via reduction of Th17, Th1 response and expansion of Tregs, and M2-polarized macrophages.

The intestinal microbiota has been increasingly recognized as an important player in normal physiology and in many pathologic processes. Although both quantitative and qualitative changes in microbiota are frequently observed in chronic inflammatory or metabolic diseases, its impact on acute illnesses such as AKI is relatively unknown.[8–10,18,19]

In this study we observed that the microbial community 1 day after IRI was already clearly distinguished from that of sham-operated mice. The hallmarks of dysbiosis included an increase in relative abundance of *Escherichia* and *Enterobacter* and decreased abundance of *Lactobacillus, Ruminococcus*, and Lachnospiraceae. Both *Enterobacter* and *Escherichia* belong to the Enterobacteriaceae family and are known as enteropathogenic bacteria producing lipopolysaccharide. A study showed the critical role of *Enterobacter cloacae* B29 as a pathogenic microbe in the development of obesity.[20] In contrast, families of Lachnospiraceae, Ruminococcaceae, and *Lacobacilli* that are well-known butyrate formers in the

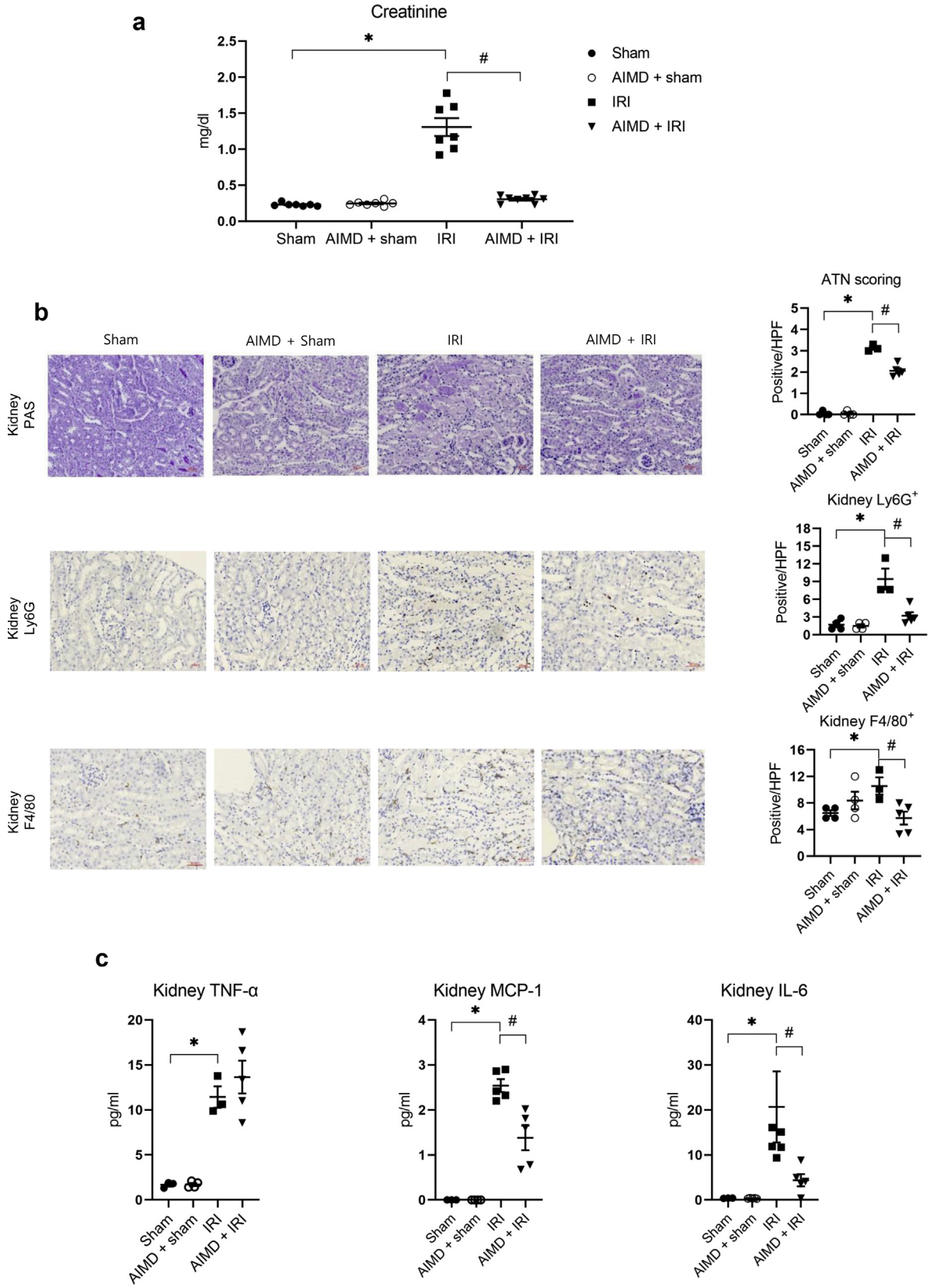

Figure 6 | Antibiotic-induced microbiota depletion (AIMD) attenuated ischemia/reperfusion injury (IRI). Mice were treated with a combination of antibiotics via oral gavage for 2 weeks before ischemia and underwent IRI. (**a**) Serum creatinine on day 1 of IRI. (**b**) Representative images of periodic acid–Schiff (PAS)–stained kidney tissue section (original magnification ×100, upper left), tubular injury score (upper right), representative images of Ly6G immunohistochemistry (original magnification ×100, middle left), the number of kidney (continued)

healthy intestine were decreased.[21,22] As expected, we found that levels of SCFAs were significantly reduced in feces of day 1 IRI mice. Butyrate has pleiotropic functions such as an energy source of colonocytes, promoting cell proliferation, immune tolerance, and barrier strengthening.[23,24] We then observed that dysbiosis induced by kidney IRI was associated with increased colonocyte apoptosis, inflammation, and altered tight junction proteins. The percentage of IL-17A$^+$ T cells, neutrophils, and $CX_3CR_1^{intermediate}$ macrophages increased, and all these changes in the intestine after kidney IRI led to increased permeability and also significantly elevated levels of endotoxin. In addition to endotoxin, we also observed the significantly increased number of bacterial 16S rRNA amplicon reads in the liver of post-IRI mice, showing the development of bacterial translocation after kidney IRI. Given that endotoxin is a pathogen-associated molecular pattern, recognized by toll-like receptors or other pattern recognition receptors, these data suggest the possible role of intestinal dysbiosis to potentiate systemic inflammation after kidney IRI.

We also found that the intestinal microbiome, inflammation, and metabolite levels showed dynamic changes during the recovery phase. Although microbiomes on days 3 and 7 after IRI showed somewhat overlapping features, they were distinctly separated from that of day 1 IRI. At the genus level, the most prominent difference was re-expansion of *Lactobacilli* with partial restoration of stool SCFAs, suggesting that microbiota during the recovery phase might also participate in the kidney recovery process. However, the significance of dynamic alteration in the intestinal microbiome after IRI needs to be further studied.

Although studies demonstrated that dysbiosis is associated with many pathologic conditions, a direct causal link between specific microbes and disease pathogenesis has not been determined. However, *Prevotella copri* and *E cloacae* B28 have been recently identified to play a causative role in the development of rheumatoid arthritis and obesity, respectively.[10,18] In our study we determined the effect of dysbiosis on AKI severity using stool transplantation in GF mice. GF mice colonized with microbiota from IRI mice developed more severe kidney injury in recipient mice compared with those colonized with microbiota from sham-operated mice, indicating that dysbiosis directly contributes to post-ischemic kidney injury. More severe kidney injury was associated with significantly higher levels of INF-γ and TNF-α in the kidneys. These results show a unique bidirectional relationship between the kidney and intestine during AKI and suggest that dysbiosis is not only the consequence of AKI but also might be one of the primary modifiers of AKI outcome.

To determine whether manipulation of microbiota affect kidney IRI, we tested the effect of AIMD in IRI. Depletion of microbiota by antibiotics led to marked protection from IRI. The beneficial effect of gut microbiota depletion in kidney IRI was previously shown by Emal *et al.*,[25] who showed that the renoprotective effect of microbiota depletion was mediated by reducing the maturation status of F4/80$^+$ renal resident macrophage and bone marrow–derived monocytes.

In our study we observed that the renoprotective effect of AIMD was associated with significant reduction of Th17 and Th1 response and also with expansion of local and systemic Tregs. IL-17 is a well-known proinflammatory cytokine, and Park *et al.*[13] showed that kidney IRI provoked small intestinal Paneth cell release of IL-17A, and genetic or pharmacologic depletion of Paneth cells decreased small intestinal IL-17A secretion, subsequently mitigating intestinal, hepatic, and kidney injury after AKI. In addition to a reduced Th17 response, AIMD was also associated with expansion of Tregs. The percentage of CD4$^+$ CD25$^+$ Tregs and Foxp3 expression in MNL, spleen, and kidney significantly increased in AIMD mice. These results are comparable with a study by Ochoa-Reparaz *et al.*,[26] who showed the expansion of Tregs in MNL and spleen after oral administration of antibiotics and suggested that this cell-mediated peripheral immune tolerance is a mechanism of protection of microbiota depletion against autoimmune encephalitis in mice.

Tregs are a subpopulation of T cells with immune modulatory function. They have been shown to counterbalance an early, overwhelmed innate immune response and also to promote repair after IRI. The critical role of Tregs has also been demonstrated in other studies showing that depletion of Tregs abolishes the renoprotective effect of immune modulatory strategies such as delayed ischemic preconditioning and heat preconditioning.[27,28] As expected, the expansion of these cells in microbiota depleted mice led to significant reductions of the proinflammatory cytokine IL-6 and chemokine monocyte chemoattractant peptide-1 levels. These data suggest that expansion of Tregs in AIMD mice partially offset an early inflammatory response in IRI. Partial mitigation or restoration of a renoprotective effect of AIMD by depletion or adoptive transfer of Tregs suggests that the AIMD-induced renoprotective effect is directly mediated by the local and systemic expansion of Tregs.

Macrophages are heterogeneous cells of substantial plasticity, and studies have demonstrated that macrophage polarization is an important regulator in both the injury and repair phases of IRI. M1 macrophages participate in initial injury by producing proinflammatory cytokines, whereas M2 macrophages dampen injury and facilitate tissue repair by

Figure 6 | (continued) Ly6G$^+$ cells (middle right), representative images of F4/80 immunohistochemistry (original magnification ×100, lower left), and the number of F4/80$^+$ cells (lower right) on day 1 of IRI. (**c**) Multiple cytokine and chemokine protein levels in kidney tissues measured by cytometric bead array (mouse inflammation kit; BD Bioscience, San Jose, CA). Symbols represent individual animals, and horizontal lines show mean values. Data are expressed as mean ± SEM. The 2-tailed unpaired *t* test was used in all graphs (4–5 per group). *$P < 0.05$ compared with the sham, #$P < 0.05$ compared with IRI. HPF, high-power field; IL, interleukin; MCP-1, monocyte chemoattractant peptide-1; TNF, tumor necrosis factor. To optimize viewing of this image, please see the online version of this article at www.kidney-international.org.

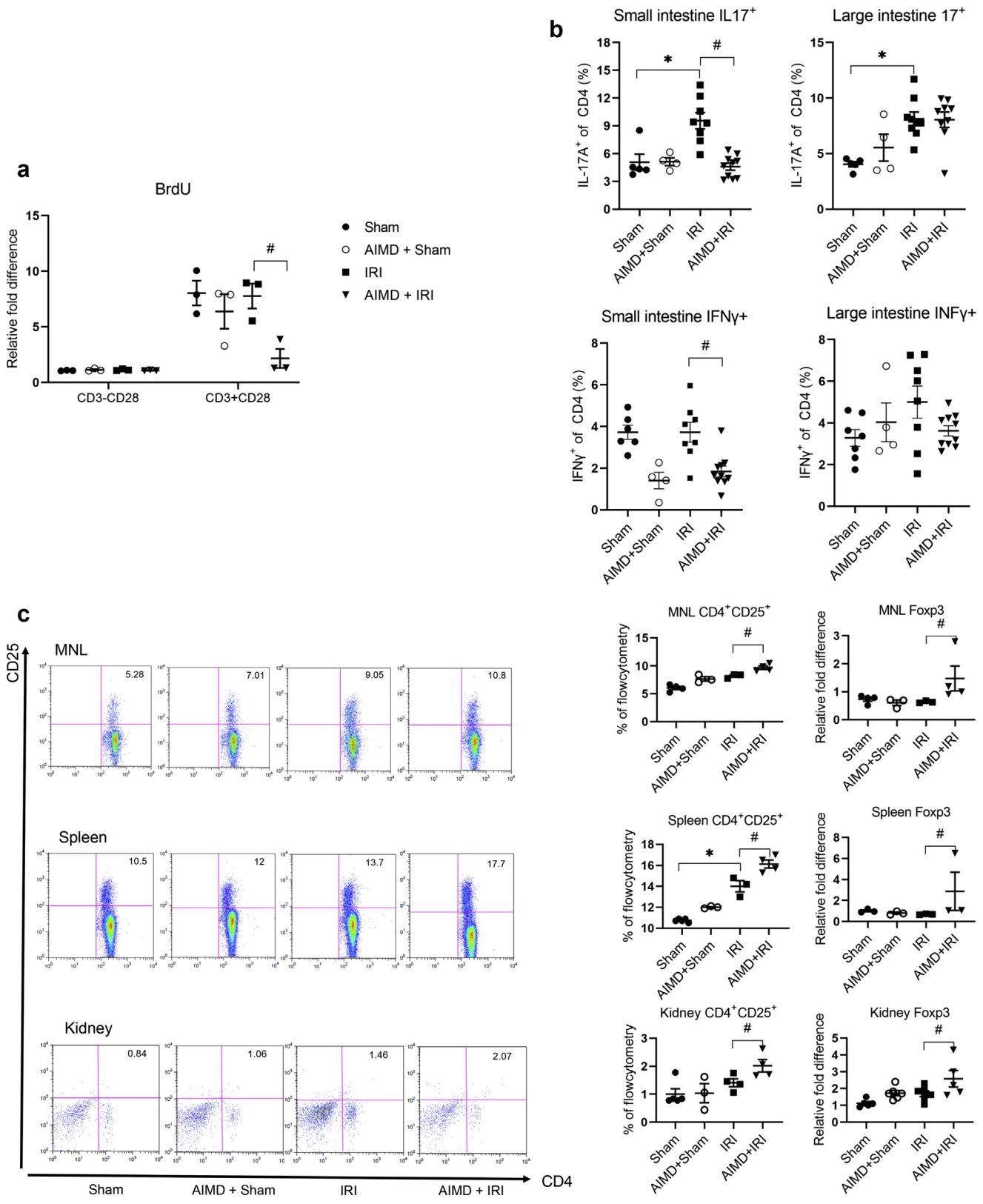

Figure 7 | Renoprotective effect of antibiotic-induced microbiota depletion (AIMD) is partially mediated by reducing T helper cell 1 (Th1), T helper cell 17 (Th17) response, and expanding regulatory T cells (Tregs). (**a**) Phenotype of mesenteric lymph node (MLN) T cells were compared. One $\times$ 10^5 cells from MLNs were cultured with or without anti-mouse CD3 Ab/anti-mouse CD28 Ab for 72 hours, and the proliferation was measured by bromodeoxyuridine (BrdU) incorporation. Fold difference compared with cells from CD3 negative plates were compared. (**b**) Flow cytometric detection of interleukin (IL)-17A$^+$ and interferon (IFN)-γ^+ CD4 cells in small and large intestines were compared (**c**) Flow-cytometric detection of CD4$^+$ CD25$^+$ Tregs; the percentage of Tregs of the total number of CD4$^+$ cells, Foxp3 mRNA expression in mesenteric (continued)

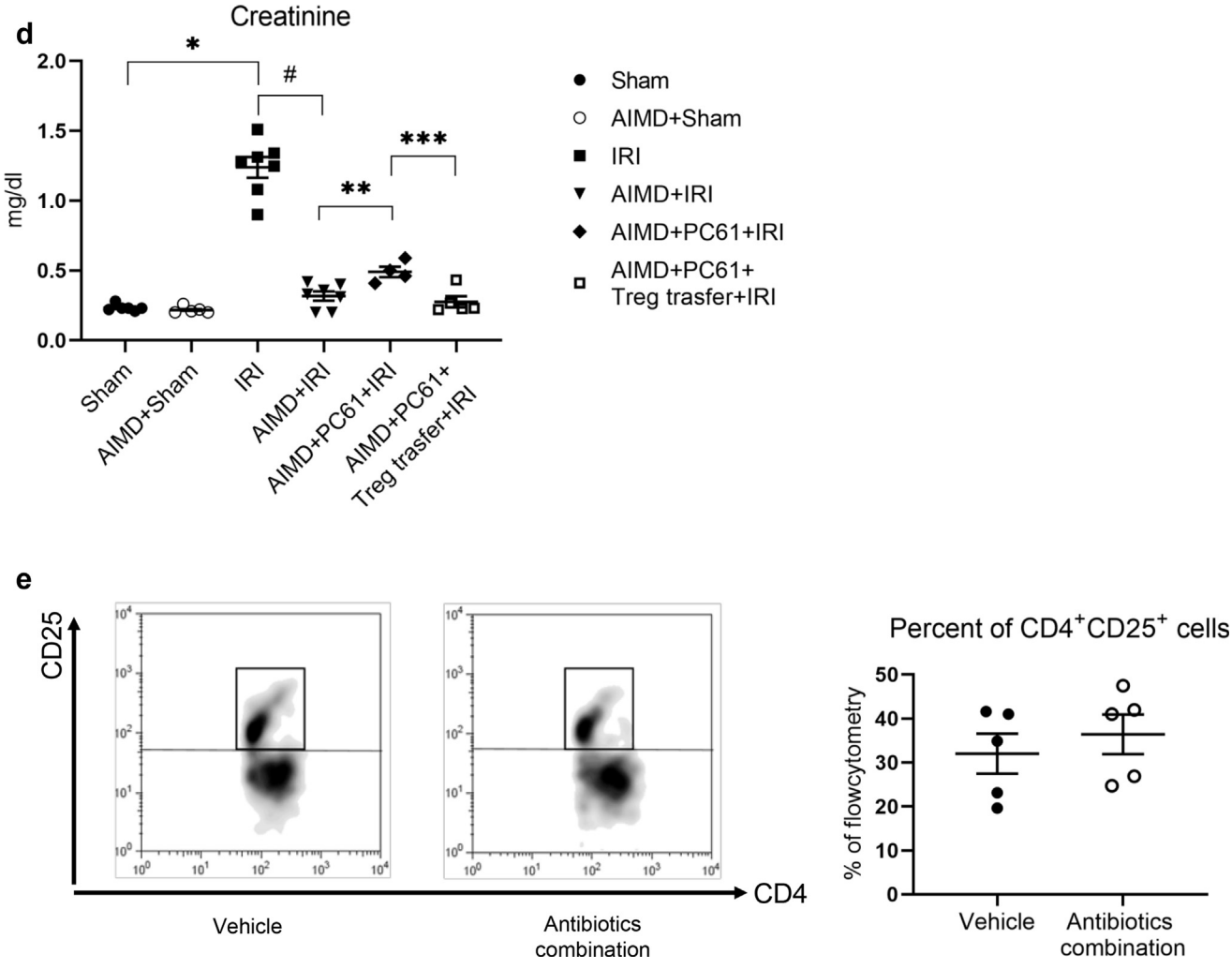

producing anti-inflammatory cytokines.[29] In our study we first observed that AIMD resulted in expansion of $Ly6^{+}$ $CX_3CR_1^{high}$ M2-like resident macrophages in the colon after IRI. Previous studies showed that $CX_3CR_1^{high}$ cells represent resident M2-like macrophages, whereas $CX_3CR_1^{intermediate}$ cells represent proinflammatory macrophages.[19] Decreased iNOS and increased arginase in the colon also suggest that AIMD induced M2 macrophage polarization in the intestinal microenvironment. However, a lack of clear distinction between macrophage and dendritic cells due to overlapping surface markers is a limitation of this study and warrants further studies. In addition to intestinal M2 polarization, we also observed the relative expansion of M2 macrophages ($F4/80^{+}$, $CD206^{+}$) in the kidneys of AIMD mice after IRI. Given that these M2 macrophages produce IL-10, which can dampen early innate immune responses, AIMD-induced M2 macrophage polarization in the colon and kidney is likely to contribute to its renoprotective effect.

Although we demonstrated the possibility that AIMD-induced changes in gut mucosal immunity toward anti-

Figure 7 | (continued) lymph nodes (upper), spleen (middle), and kidney (lower) were compared. (**d**) To examine the role of Tregs in renoprotective effect of AIMD, Tregs were depleted by using anti-mouse CD25 monoclonal antibodies (PC61; BioLegend, San Diego, CA) administered 10 and 5 days before ischemia/reperfusion injury (IRI). For adoptive transfer, 2×10^5 $Foxp3^{+}$ cells were i.v. injected 3 days before IRI, and serum creatinine was measured on day 1 of IRI. (**e**) One $\times$ 10^5 cells from MLNs were cultured with combination of neomycin, metronidazole, ampicillin, and vancomycin for 72 hours, and the percentage of $CD4^{+}$ $CD25^{+}$ cells was compared. Symbols represent individual animals, and horizontal lines show mean values. Data are expressed as mean ± SEM. The 2-tailed unpaired *t* test was used in all graphs (3–5 per group). *$P < 0.05$ sham versus IRI, #$P < 0.05$ IRI versus AIMD+IRI, **$P < 0.05$ AIMD+IRI versus AIMD+PC61+IRI, ***$P < 0.05$ AIMD+PC61+IRIversu AIMD+PC61+Treg (adoptive transfer)+IRI.

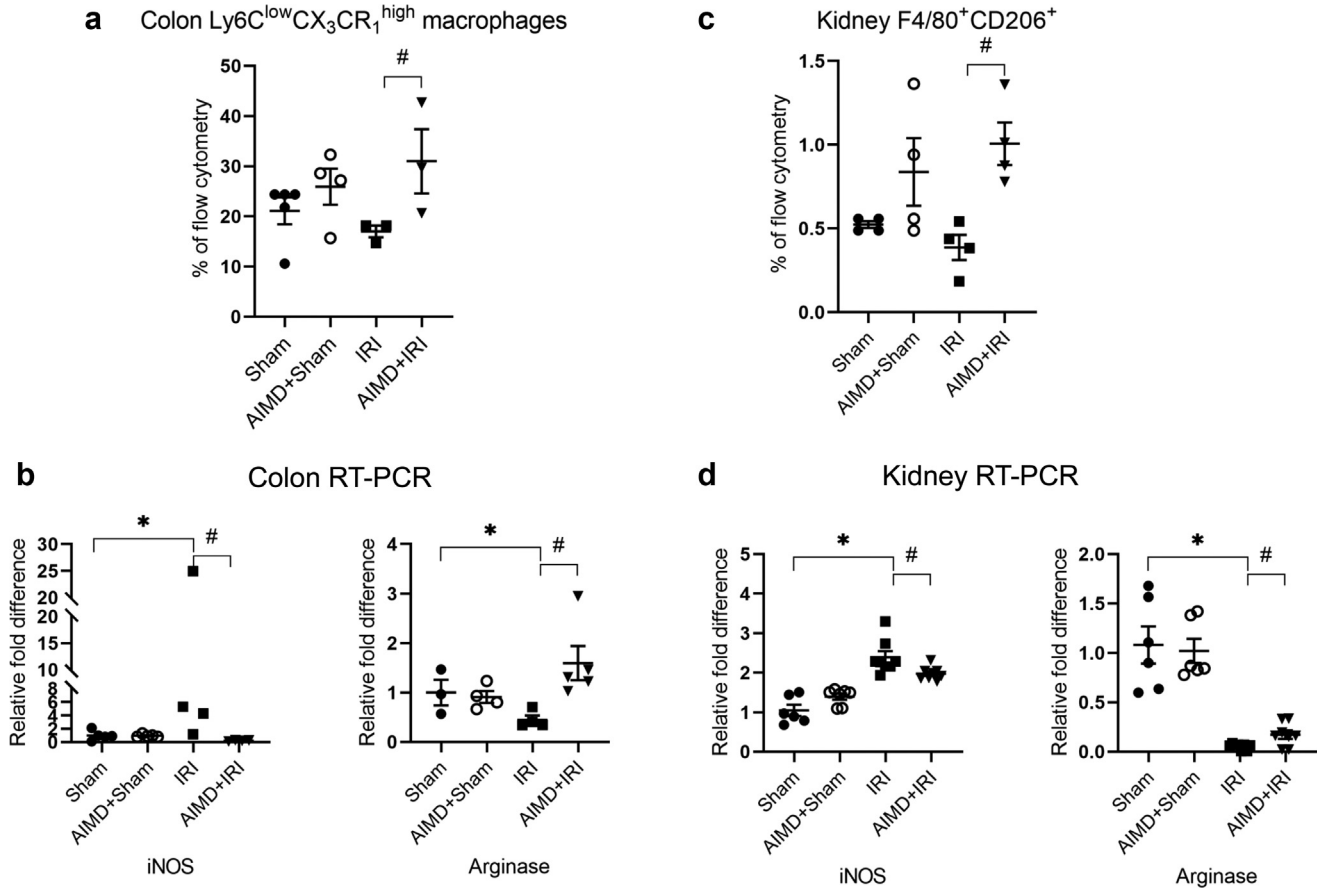

Figure 8 | Antibiotic-induced microbiota depletion (AIMD)–induced renoprotective effect is partially mediated by expansion of M2 macrophages. (**a**) Flow cytometric detection of Ly6c$^+$CX$_3$CR$_1$$^+$ colon macrophages on day 1 of ischemia/reperfusion injury (IRI). Percentage of Ly6c^{low}CX$_3$CR$_1$^{high} resident macrophages were compared. (**b**) Reverse transcriptase-polymerase chain reaction (RT-PCR) analysis of colon-inducible nitric oxide synthase (iNOS) and arginase. (**c**) Flow cytometric detection of F4/80$^+$ CD206$^+$ M2 macrophages in the kidney. Percentage of F4/80$^+$ CD206$^+$ macrophages was compared. (**d**) RT-PCR analysis of kidney iNOS and arginase. Symbols represent individual animals, and horizontal lines show mean values. Data are expressed as mean ± SEM. The 2-tailed unpaired *t* test was used in all graphs (3–8 per group) *$P < 0.05$ sham versus IRI, #$P < 0.05$ IRI versus AIMD+IRI.

inflammation and tolerance lead to renoprotective effects against kidney IRI, it is not clear whether these M2 macrophages or Tregs from the intestine actually egress and directly migrate to injured kidneys. However, recent studies using Kaede transgenic mice that universally express a photoconvertible fluorescent reporter showed that gut-derived T cells could easily traffic to the spleen.[30] Another study by Singh *et al.*[31] also demonstrated that T cells and monocytes that were fluorescently labeled by microinjection to Peyer's patch were found in the ischemic hemisphere in a mouse model of stroke. These results suggest that AIMD-induced expansion of Tregs and M2 macrophages in the intestine can egress from the intestines and subsequently traffic into injured kidneys to exert their beneficial effect after IRI.

Although our study demonstrated the possible important contribution of intestinal dysbiosis, T cells, and macrophages in kidney IRI, the intestine also harbors large numbers of B cells or dendritic cells that also participate in balancing the immune response. The number of IgA producing plasma cells in the intestine exceeds that in the rest of body, and secretory IgA is important in maintaining barrier integrity. Lamina propria dendritic cells extends their dendrites into the lumen and patrolling luminal environment and play an important role in shaping the adaptive immune response. Regarding the differential role of various types of immune cells in the intestine after kidney IRI, more studies are needed.

In conclusion, our study demonstrated a novel concept that intestinal dysbiosis is a consequence of kidney IRI and is also an important modifier of post-ischemic kidney outcome by immune modulatory effects. Microbiota depletion before injury provided short-term renoprotective effects against IRI, and this effect was mediated by reduction of Th17 and Th1 response and by expansion of Tregs and M2 macrophages. The restoration of healthy microbiota in the intestine might therefore provide a novel preventive or therapeutic strategy for AKI.

METHODS

Experimental animals and renal IRI

Six- to 8-week-old male C57BL/6 mice (Orient Bio Inc, Seoul, Korea) were housed in a specific pathogen-free (SPF) facility under a 12-hour light–dark cycle with free sterile feed and distilled water. GF C57BL/6 mice were housed in a positive pressured isocage system at Pohang University of Science and Technology (POSTECH) animal care facility. All experimental protocols were approved by the animal care committee of Korea University and POSTECH (IRB No. KOREA-2018-0094 and POSTECH-2019-0017), complied with the National Institutes of Health guide for the care and use of laboratory animals, and followed the National Research Council publication, *Guide for the Care and Use of Laboratory Animals, 8th Edition*.[32] To induce IRI, mice were subjected to bilateral renal pedicle clamping for 25.5 minutes (SPF mice) and for 28.5 minutes (GF mice) by flank incision. After the clamps were removed, reperfusion of the kidneys was observed. A sham operation was performed in a similar manner, except the renal pedicles were clamped. For depletion of Tregs, rat anti-mouse CD25 monoclonal antibodies (PC61; BioLegend, San Diego, CA) were administered intraperitoneally to C57BL/6 mice at a dose of 0.25 mg per mice 10 and 5 days before IRI. For adoptive transfer of Tregs, cells from spleen and MNL of Foxp3-GFP mice were isolated and stimulated with IL-2 for 48 hours. GFP^+ cells (purity $>$ 98%) were sorted by using BD FACSAria III (BD Biosciences, San Jose, CA), and then 5×10^5 cells were adoptively transferred via tail vein injection into Treg-depleted AIMD mice 3 days before IRI.

Fecal microbiota reconstitution and AIMD

Fresh feces obtained on day 1 of sham and IRI mice were resuspended in 0.9% normal saline (0.2 g/ml). Two hundred microliter of this soup was administrated via oral gavage on days 0 and 10 to GF B6 mice. Microbiota-reconstituted mice were housed under an isocage system, and IRI was induced on day 21. For depletion of intestinal microbiota, a group of SPF mice was treated with a mixture of 4 broad-spectrum antibiotics (neomycin 25 mg/kg [Sigma Aldrich Korea, Seoul, Korea], metronidazole 25 mg/kg [JW Pharmaceutical, Seoul, Korea], ampicillin 60 mg/kg [Youngjin Pharmaceutical, Seoul, Korea], and vancomycin 400 mg/kg [CJ Healthcare, Seoul, Korea]) via oral gavage for 2 weeks before IRI.

Microbiome analysis

For intestinal microbiome analysis, feces of mice were collected in a sterile microtube and stored in a –70 °C freezer until analysis. To assess the bacterial translocation, MNL or liver tissue was also collected with using aseptic technique. DNA was isolated from the feces, MNL, and liver using the FastDNA SPIN Kit for soil (MP Biomedicals, Irvine, CA). Thermal cycling was performed with the CFX 96 Real-Time system (Bio-Rad, Hercules, CA) by using Dr. Max DNA polymerase (MGmed, Seoul, Korea) with the following cycling conditions: initial denaturation at 95 °C for 3 minutes; 8 cycles of denaturation at 95 °C for 30 seconds, annealing at 55 °C for 30 seconds, and extension at 72 °C for 30 seconds; final extension at 72 °C for 5 minutes. The amplified PCR products were purified with CleanPCR (CleanNA, Waddinxveen, Netherlands). The quality assessment was done on a Bioanalyzer 2100 (Agilent, Palo Alto, CA) using a DNA 7500 chip. The amplicons were pooled for sequencing with Illumina MiSeq Sequencing system (Illumina, San Diego, CA) according to the manufacturer's instructions. The EzBioCloud system provided quantitative analysis that clustered into OTUs and searches against the ExTaxon database at ChUNLAB (Seoul, Korea). Microbial richness was assessed by the number of OTUs, ACE, and Chao-1 indices. Diversity was assessed by the Shannon diversity index. To examine the difference between the whole microbial communities, sequence data were normalized at 20,000 read number per samples, and then the principal coordinates analysis was performed on the Jensen-Shannon distance.

Measurement of SCFAs

Mouse fecal samples were homogenized, and the clear supernatant was used for measurement of SCFAs by liquid chromatography tandem mass spectrometry in multiple reaction monitoring mode (Seoul National University National Instrumentation Center for Environmental Management, Seoul, Korea).

Intestinal permeability

Intestinal permeability was measured by using fluorescein isothiocyanate conjugated dextran (FITC-dextran, catalog number FD4; Sigma-Aldrich, St. Louis, MO). Briefly, FITC-dextran dissolved in phosphate-buffered saline (PBS; 100 mg/ml) was given by oral gavage (44 mg/100 g) after overnight water starvation, and FITC fluorescein activity in the blood was measured at 4 hours. This protocol is based on Bio-protocol (http://www.bio-protocol.org/e1289).

Flow cytometry

Flow cytometric analyses of leukocytes in the MNL, spleen, kidney, and intestine were performed. Cells were stained with fluorochrome-labeled monoclonal antibodies (CD45, F4/80, CD206, CX_3CR_1, Ly6C, CD4, CD25, 7-aminoactinomycin D; eBioscience, BioLegend, and BD Biosciences), and only 7- aminoactinomycin D–negative viable cells were read by a 4-color flow cytometry (FACSCaliburTM; BD Bioscience) device and analyzed by FlowJo (Tree Star Inc., Ashland, CA).

Percentage of $IL\text{-}17A^+$ or $IFN\text{-}\gamma^+$ CD4 T cells were analyzed by intracellular cytokine staining. Isolated cells were stimulated by phorbol 12-myristate 13-acetate (1 mol/l) and ionomycin (1 mol/l) in the presence of Golgi-Stop (554724; BD Biosciences) for 4 hours. At the end of cell stimulation, cells were washed with PBS and stained with Fixable Viability Dye (Invitrogen, Carlsbad, CA) to label dead cells. Cells were washed with PBS, stained with anti-CD4 (RM4-5), and then fixed with Foxp3 Fix/Perm Buffer and washed with Perm Buffer according to the manufacturer's protocol (eBioscience, San Diego, CA) . Cells were then stained with anti-IL-17A (TC11-18H10.1, Biolegend) and anti-IFN-γ (XMG1.2, Biolegend), washed, and resuspended in PBS. Cell acquisition was performed on LSR Fortessa (BD Biosciences), and data were analyzed using FlowJo software suite.

Real-time reverse transcription-PCR

For detection of TNF-α, IFN-γ, iNOS, arginase, IL-6, IL-10, and Foxp3 mRNA expression, total RNA was purified by TRIzol extraction (Thermo Fisher Scientific, Waltham, MA) according to the manufacturer's protocol, and cDNA was synthesized using standard procedures. Real-time PCR was performed in iCycler IQ Real-Time PCR Detection System (Bio-Rad Laboratories, Hercules, CA) with using the iQ SYBR Green Supermix (Bio-Rad, Hercules, CA) for Foxp3 or TaqMan PCR Master Mix (Applied Biosystems, Foster City, CA) for the others. We used ribosomal 18S as the reference gene (RT2 PCR Primer Set; Applied Biosystems) and fold difference compared with sham was compared.

Western blot analysis

Proteins were extracted from whole colon tissue using the bicinchoninic acid method, and expression of tight junction proteins were examined using anti-mouse antibodies of claudin-1 (1:200, ab15098; Abcam, Cambridge, MA) and claudin-2 (1:400, ab125293; Abcam). Band intensities were measured by Image Pro (Image Studio Lite LI-COR Biosciences, Lincoln, NE) software and normalized by β-actin.

Quantification of cytokines, chemokine, and endotoxin

Cytokines and chemokines in the kidney and colon were quantified by cytometric bead array using a mouse inflammation kit (BD Biosciences) according to the manufacturer's instructions. Mouse gram-negative endotoxin ELISA kit (competitive EIA, LS-F28324, LSBio, Seattle, WA) was used for the measurement of serum endotoxin level.

Histologic analysis

Tubular injury was semiquantitatively assessed in periodic acid–Schiff stained kidney tissues. For detection of monocytes/macrophages or neutrophils, formalin-fixed and paraffin-embedded kidney and colon were stained with monoclonal antibody against F4/80 (1:100, mch-497-GA; Bio-Rad) or Ly6G (1:200, 14-59-85; eBioscience). The mean number of positive cells per 8 to 10 high-power fields was compared. Colon epithelial cell apoptosis was quantified by counting terminal deoxynucleotidyl transferase dUTP nick end labeling–positive epithelial cells in 8 to 10 high-power fields (×200).

In vitro analysis

To assess T-cell function, 1×10^5 MNL cells per well were cultured in the presence of mouse anti-CD3 and anti-CD28 Abs (BD BioCoatTM Mouse T-cell Activation Plates; BD Biosciences) for 48 hours, labeled with BrdU for 18 hours, and the amount of BrdU incorporated was determined. Fold difference compared with that of CD3 negative plate was compared.

To examine the direct effect of antibiotics on Treg expansion, 1×10^5 MNL cells were incubated with the antibiotics mixture, and the percentage of $CD4^+$ $CD25^+$ cells were measured at 72 hours. The antibiotic mixture regimen was the same as that used in mice.

Statistical analysis

Data were analyzed using GraphPad Prism version 8.0 (GraphPad Software, San Diego, CA). Data are presented as individual symbols, and mean values are expressed as horizontal lines. An unpaired *t* test and analysis of variance (with Bonferroni post-test) were used for comparisons between 2 and 3 or more groups, respectively. A $P < 0.05$ was considered statistically significant.

DISCLOSURE

All the authors declared no competing interests.

ACKNOWLEDGMENTS

This study was supported by the Basic Science Research Program through the National Research Foundation of Korea funded by the Ministry of Education (2017R1A2B1002734).

AUTHOR CONTRIBUTIONS

JHY, SHI, and SKJ designed the study. JHY, YSG, HYL, and CJK carried out experiments. JHY, M-GK, SWO, WYC, SHI, and SKJ analyzed the data. JHY, M-GK, WYC, and SKJ drafted and revised the manuscript. All authors approved the final version of the manuscript.

SUPPLEMENTARY MATERIAL

Supplementary File (PowerPoint)

Figure S1. Effect of antibiotic-induced microbiota depletion (AIMD) on colon inflammation, apoptosis, and intestinal permeability. (**A**) Representative images of colon apoptosis, deoxynucleotidyl transferase dUTP nick end labeling (TUNEL), ×200. The number of $TUNEL^+$ apoptotic colonocytes are shown (top). Representative images of Ly6G immunohistochemistry, ×200, the number of kidney $Ly6G^+$ cells (middle), and the representative images of F4/80 immunohistochemistry, ×200, the number of $F4/80^+$ cells (bottom). (**B**) Western blot of claudin-1, claudin-2, β-actin, and band intensities normalized to β -actin were compared. (**C**) Intestinal permeability was measured by detecting fluorescein activity of fluorescein isothiocyanate conjugated (FITC) 4 hours after oral administration of FITC-dextran on day 1 of IRI. Symbols represent individual animals, and horizontal lines show mean values. Data are expressed as mean ± SEM. The 2-tailed unpaired *t* test was used in all graphs (3–4 per group). $^*P < 0.05$ compared with sham, $\#P < 0.05$ compared with IRI.

REFERENCES

1. Fuhrman DY, Kane-Gill S, Goldstein SL, et al. Acute kidney injury epidemiology, risk factors, and outcomes in critically ill patients 16-25 years of age treated in an adult intensive care unit. *Ann Intens Care*. 2018;8:26.
2. Lewington AJP, Cerdá J, Mehta RL. Raising awareness of acute kidney injury: a global perspective of a silent killer. *Kidney Int*. 2013;84:457–467.
3. Doyle JF, Forni LG. Acute kidney injury: short-term and long-term effects. *Crit Care*. 2016;20:188.
4. Coca SG, Yusuf B, Shlipak MG, et al. Long-term risk of mortality and other adverse outcomes after acute kidney injury: a systematic review and meta-analysis. *Am J Kidney Dis*. 2009;53:961–973.
5. Doi K, Rabb H. Impact of acute kidney injury on distant organ function: recent findings and potential therapeutic targets. *Kidney Int*. 2016;89:555–564.
6. Savage DC. Microbial ecology of the gastrointestinal tract. *Annu Rev Microbiol*. 1977;31:107–133.
7. Marchesi JR, Adams DH, Fava F, et al. The gut microbiota and host health: a new clinical frontier. *Gut*. 2016;65:330–339.
8. Abdollahi-Roodsaz S, Abramson SB, Scher JU. The metabolic role of the gut microbiota in health and rheumatic disease: mechanisms and interventions. *Nat Rev Rheumatol*. 2016;12:446–455.
9. Maeda Y, Kurakawa T, Umemoto E, et al. Dysbiosis contributes to arthritis development via activation of autoreactive T cells in the intestine. *Arthritis Rheumatol*. 2016;68:2646–2661.
10. Alpizar-Rodriguez D, Lesker TR, Gronow A, et al. *Prevotella copri* in individuals at risk for rheumatoid arthritis. *Anne Rheum Dis*. 2019;78:590–593.
11. Kelsall B. Recent progress in understanding the phenotype and function of intestinal dendritic cells and macrophages. *Mucosal Immunol*. 2008;1:460–469.
12. Manzano M, Abadía-Molina AC, García-Olivares E, et al. Absolute counts and distribution of lymphocyte subsets in small intestine of BALB/c mice change during weaning. *J Nutr*. 2002;132:2757–2762.
13. Park SW, Chen SWC, Kim M, et al. Cytokines induce small intestine and liver injury after renal ischemia or nephrectomy. *Lab Invest*. 2011;91:63–84.
14. Andrade-Oliveira V, Amano MT, Correa-Costa M, et al. Gut bacteria products prevent AKI induced by ischemia-reperfusion. *J Am Soc Nephrol*. 2015;26:1877–1888.
15. Vijay-Kumar M, Chassaing B, Kumar M, et al. Mammalian gut immunity. *Biomed J*. 2014;37:246.
16. Zeng MY, Inohara N, Nuñez G. Mechanisms of inflammation-driven bacterial dysbiosis in the gut. *Mucosal Immunol*. 2017;10:18–26.
17. Zununi Vahed S, Barzegari A, Zuluaga M, et al. Myocardial infarction and gut microbiota: an incidental connection. *Pharmacol Res*. 2018;129:308–317.
18. Maeda Y, Takeda K. Role of gut microbiota in rheumatoid arthritis. *J Clin Med*. 2017;6:60.
19. Yang J, Lim SY, Ko YS, et al. Intestinal barrier disruption and dysregulated mucosal immunity contribute to kidney fibrosis in chronic kidney disease. *Nephrol Dial Transplant*. 2019;34:419–428.

20. Fei N, Zhao L. An opportunistic pathogen isolated from the gut of an obese human causes obesity in germfree mice. *ISME J*. 2013;7:880–884.
21. Biddle A, Stewart L, Blanchard J, Leschine S. Untangling the genetic basis of fibrolytic specialization by Lachnospiraceae and Ruminococcaceae in diverse gut communities. *Diversity*. 2013;5:627–640.
22. Tsukahara T, Hashizume K, Koyama H, Ushida K. Stimulation of butyrate production through the metabolic interaction among lactic acid bacteria, *Lactobacillus acidophilus*, and lactic acid-utilizing bacteria, *Megasphaera elsdenii*, in porcine cecal digesta. *Animal Sci J*. 2006;77:454–461.
23. Hamer HM, Jonkers D, Venema K, et al. Review article: the role of butyrate on colonic function. *Aliment Pharmacol Therap*. 2008;27:104–119.
24. Leonel AJ, Alvarez-Leite JI. Butyrate: implications for intestinal function. *Curr Opin Clin Nutr Metab Care*. 2012;15:474–479.
25. Emal D, Rampanelli E, Stroo I, et al. Depletion of gut microbiota protects against renal ischemia-reperfusion injury. *J Am Soc Nephrol*. 2017;28:1450–1461.
26. Ochoa-Reparaz J, Mielcarz DW, Ditrio LE, et al. Central nervous system demyelinating disease protection by the human commensal *Bacteroides fragilis* depends on polysaccharide A expression. *J Immunol*. 2010;185:4101–4108.
27. Kim M-G, Jung Cho E, Won Lee J, et al. The heat-shock protein-70–induced renoprotective effect is partially mediated by CD4 + CD25 + Foxp3 + regulatory T cells in ischemia/reperfusion-induced acute kidney injury. *Kidney Int*. 2014;85:62–71.
28. Kim M-G, Koo TY, Yan J-J, et al. IL-2/anti-IL-2 complex attenuates renal ischemia-reperfusion injury through expansion of regulatory T cells. *J Am Soc Nephrol*. 2013;24:1529–1536.
29. Jo S-K, Sung S-A, Cho W-Y, et al. Macrophages contribute to the initiation of ischaemic acute renal failure in rats. *Nephrol Dialysis Transplant*. 2006;21:1231–1239.
30. Jarick KJ, Mokhtari Z, Scheller L, et al. Photoconversion of alloreactive T cells in murine Peyer's patches during acute graft-versus-host disease: tracking the homing route of highly proliferative cells in vivo. *Front Immunol*. 2018;9:1468.
31. Singh V, Roth S, Llovera G, et al. Microbiota dysbiosis controls the neuroinflammatory response after stroke. *J Neurosci*. 2016;36:7428–7440.
32. National Research Council (Us) Committee for the Update of the Guide for the Care and Use of Laboratory Animals. Guide for the Care and Use of Laboratory Animals, 8th Edition. Washington, DC: The National Academies Press; 2011. Available at: https://grants.nih.gov/grants/olaw/guide-for-the-care-and-use-of-laboratory-animals.pdf. Accessed August 13, 2020.